IUST International Journal of Engineering Science, Vol.17 , No.3-4 , 2006, Page **37-46**

Numerical Study of Hemodynamic Wall Parameters on Pulsatile Flow through Arterial Stenosis

M.R. Modarres Razavi, S.H. Seyedein and P.B. Shahabi

Abstract: In this paper hemodynamic wall parameters which play an important role to diagnose arterial disease were studied and compared for three different rheology models (Newtonian, Power law and Quemada). Also because of the pulsatile behavior of blood flow the results were obtained for three Womersley numbers which represent the frequencies of the applied pulses. Results show that Quemada model always located between Newtonian and Power law models however its behavior is closer to Power law model. Concerning this behavior and better agreement between Quemada and experimental blood viscosity, it can be expected that Quemada results are more realistic and accurate.

Keywords: Pulsatile flow, non-Newtonian fluid, Hemodynamic wall parameter, Stenosis, Womersley number

1. Introduction

The main goal of blood flow simulation in vessels is to evaluate hemodynamic forces which artery wall experiences due to different factors like the pulsatile blood flow, the fluid flow geometry and the blood rheology behavior (Quasi-Newtonian or non-Newtonian fluid). Besides, it is important to know if there is any observable correlation between flow pattern characteristics and abnormal biological events and arterial diseases like stenosis, thrombosis and atherosclerosis.

It is proved that hemodynamic parameters play fundamental roles in the regulation of vascular biology and access of arterial diseases [1]. Wall shear stress, particle residence time, recirculation zones and arterial wall strain are examples of hemodynamic parameters. Formations of dysfunctions in vascular biology are results of irregular variation of these parameters [1,2]. For example high shear stress regions, long particle residence time and low oscillatory shear stress are some cases which lead to abnormal events and finally blood vessel diseases [3].

Among various researches have been done in this field, evaluation of blood flow in stenosed vessels is one of the extraordinary subjects has been raised by many researchers. Since the arterial stenosis is one of the most widespread diseases in human beings, these researches are shown to be more valuable to scholars [4].

Received by the editor May, 9, 2005; final revised: November, 5, 2005.
M.R. Modarres Razavi is with the Department of Mechanical Eng., Ferdowsi University of Mashhad, m-razavi@ferdowsi.um.ac.ir
S.H. Seyedein, Department of Metallurgy Eng., Science & Technology University of Iran., Tehran, Iran. seyedein@iust.ac.ir
P.B. Shahabi is with the Department of Mechanical Eng., Islamic Azad University of Mashhad,pbshahabi@yahoo.com

Both experimental and computational studies have been performed to investigate blood flow in stenosed vessels [4-16]. Tu and Deville [4] used four rheological models to simulate pulsatile blood flow through arterial stenosis. They computed axial velocity, pressure variation and wall shear stress for a 75% stenosed vessel and showed that the rheological properties of blood can significantly affect the flow patterns. Ojha et al. [5] used a photochromic tracer method to record pulsatile flow velocity profiles in an experimental work. In this work both axisymmetric and asymmetric stenosis with different area reductions were analyzed and the wall shear stress variations were examined.

Kumar and Naidu [6] simulated a pulsatile suspension flow in a stenosed vessel numerically.

They showed the occurrence of recirculation regions both in upstream and downstream to the stenosis. Siouffi et al. [7] presented a study of a post-stenotic velocity flow field corresponding to the oscillatory, pulsatile physiological flow waveforms and too much emphasis was placed on the analysis of the experimental velocity-profile patterns.

They proved that beyond the influence of the flow parameters such as the Reynolds number and frequency parameter, the velocity profile (hence the wall shear stress) highly depends on the waveform. Deplano and Siouffi [9] accomplished an experimental and numerical investigation on pulsatile flows through stenosis and also they focused on the wall shear stress analysis.

They concluded that the presence of the stenosis leads to the artery acting in a direction which is opposite of a healthy artery. Buchanan et al. [10] considered rheological effects on pulsatile hemodynamics in a stenosed tube. They reported that different flow patterns formed for the highest Womersley number under

consideration ($Wo = 12.5$). The hemodynamic wall parameters and the particle residence time have been computed in this study.

Ishikawa et al. [11] examined vortex enhancement in blood flow through stenosed and locally expanded tubes. They found that vortex formation can be influenced by the frequency of pulsation in manner that the vortex in downstream of stenosis or expansion part becomes strongest at a certain frequency.

Chakravarty and Mandal [12] introduced an improved shape of the time-variant overlapping stenosis to study two-dimensional blood flow in tapered arteries with the presence of stenosis.

Long et al. [13] simulated pulsatile blood flow in three axisymmetrical and three symmetrical stenosed tube models with area reduction of 25%, 50% and 75%. They focused on the flow separation zone (FSZ) and the wall shear stress (WSS) distributions for all models.

In recent years some researchers which especially studied hemodynamic parameters include Buchanan et al. [1], Kute and Vorp [2] and Hyun et al [3].

In our previous works [15-16] the pulsatile blood flow through a stenosed tube was simulated for three different pulsation frequencies by using the Power law model for blood rheology simulation.

It was showed that the frequency of pulsation has a remarkable effect on the flow field and changes the time point and location of the vortex formation distal to the stenosis.

In present study three rheology models are considered to simulate blood rheology (Newtonian, Power law and Quemada).

These three models are compared with the computed hemodynamic parameters at three Womersley numbers for pulsatile blood flow through a stenosed tube. Of all hemodynamic parameters which computed in blood flow analysis of stenosed vessels, the wall shear stress and its derivatives are the most important ones which are examined in this study.

2. Physical Model

The schematic of local stenosis and some biological information are shown in Fig. 1.

As shown in this figure the constriction (stenosis) has no uniform profile and it is usually approximated by sinusoidal or exponential profiles [4].

In this study the following sinusoidal extension is used to determine the tubular geometry by radius r_0 and the local, smooth and axisymmetric constriction [4].

$$R(z) = \frac{r(z)}{r_0} = \begin{cases} 1 - \dfrac{d}{2}\left[1 + \cos\left(\dfrac{p\, z}{z_0}\right)\right] & if \quad |z| \le z_0 \\ 1 & if \quad |z| > z_0 \end{cases} \qquad (1)$$

Where, r_0 is the tube radius, z_0 is the stenosis half-length and d is the tube constricted thickness.

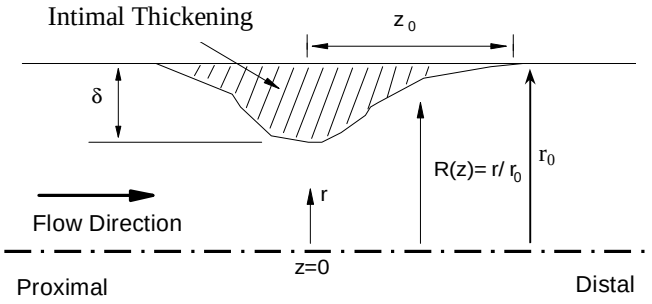

Fig. 1. Constricted Tube Schematic.

A control volume mesh of the flow field is shown in Fig. 2. As can be seen in Fig. 2 the mesh size varies in r direction, from center line to wall, and z direction, from each sides of the tube to the stenosis center, as near the wall and around the stenosis fine meshes have been generated. Therefore, with this mesh structure (300×30), velocity gradient near the wall and flow pattern components around the area reduction can be computed more accurately.

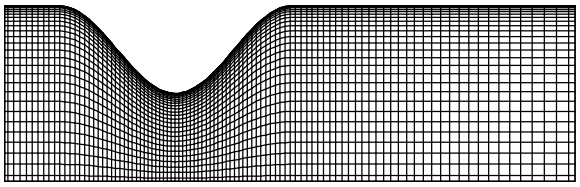

Fig. 2. Finite Volume Grid Structure of Flow Pattern.

Because of flexibility and wide use in both numerical and experimental studies a sinusoidal pulse is used for input flow. Selected relation that controls the Reynolds number is [9]:

$$Re = Re_{mean} + Re_{amp} \sin\left(2p\, \frac{t}{T}\right) \qquad (2)$$

where T is a period time. The flow input pulse and key times are shown in Fig. 3.

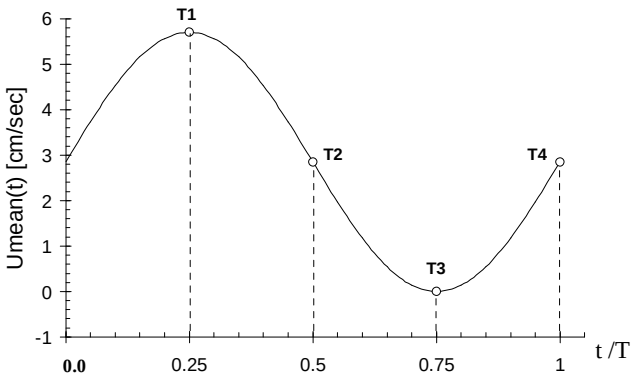

Fig. 3. Flow Input Pulse and Four Key Times.

The Reynolds number definition is based on constant tube diameter, the area-averaged velocity and blood Newtonian viscosity, i.e.

$$Re = \frac{r U D}{m_\infty} \tag{3}$$

The related viscosity to upper shear rate limit for non-Newtonian models is m_∞ and it is called the limiting high shear rate Newtonian viscosity.
It means that after this limit, blood behaves like a Newtonian fluid and non-Newtonian models should reach the Newtonian viscosity.
A dimensionless parameter called Womersley number is usually defined for periodic and pulsatile flow problems which represents pulse frequency. The Womersley number is the ratio of transient inertial effects to viscous effects with the following definition [1].

$$Wo = r_0 \left(\frac{2p}{nT} \right)^{1/2} \tag{4}$$

Where r_0 is the tube constant radius and n is the kinematic viscosity that is Newtonian viscosity, $n = m_\infty / r$ .defined based on the

3. Fluid Rheology

Nowadays, it is well-defined that blood is a non-Newtonian fluid [4,8,11,17-19]. In this study three fluid rheology, including the Newtonian, the Power law and the Quemada models are considered. For the Newtonian model viscosity is constant.
On the other hand, viscosity in non-Newtonian models varies with shear rate. The Power law model uses the following simple non-linear expression in the form of an apparent viscosity [20-22].

$$h = m \dot{g}^{n-1} \tag{5}$$

Where m and n are constitutive coefficients and constant for each fluid. Whereas blood is known as a shear-thinning fluid, thus $n < 1$.
The Quemada model defines the apparent viscosity with the following correlation [10].

$$h = \left(\sqrt{h_\infty} + \frac{\sqrt{t_0}}{\sqrt{l} + \sqrt{\dot{g}}} \right)^2 \tag{6}$$

Three constitutive coefficients are appeared in this correlation ($h_\infty ; t_0$ and l).
The additional coefficient, l , is the shear rate modifier which prevents the singularity and computation of unreal viscosity when shear rate approaches zero and increases the accuracy of the model, specially at low shear rate ranges. Constitutive coefficients of three models for human blood used in this study are listed in Table 1.
The shear rate ($\dot{g}$) which is appeared in the apparent viscosity formulation is taken as the second scalar invariant of the rate of strain tensor [23].

Table. 1. Constitutive Coefficients for Three Rheological Models.

Newtonian model	$h_N = m_\infty = 0.0309 \quad g/cm.s$
Power law model	$m = 0.1260 \quad g/cm.s^n$ $n = 0.8004$
Quemada model	$h_\infty = 0.02654 \quad g/cm.s$ $t_0 = 0.04360 \quad g/cm.s^2$ $l = 0.02181 \quad s^{-1}$

It is well known that blood has a limiting Newtonian viscosity at elevated shear rates, so the Newtonian viscosity is chosen as the lower viscosity limit for both non-Newtonian models. Each of the models reaches this limit at different shear rates. The Quemada model reaches the Newtonian limit at $\dot{g}_{max} = 256.7\ s^{-1}$, but the Power law model reaches at $\dot{g}_{max} = 76.8\ s^{-1}$ [10].
The Quemada model has lower shear rate limit viscosity ($(\sqrt{h_\infty} + \sqrt{t_0}/\sqrt{l})^2$), so it doesn't need lower bound. On the other hand, to increase the Power law model accuracy it needs to have lower bound and for blood rhelogical data the lower bound is $\dot{g}_{min} = 10^{-1}\ s^{-1}$ [10]. Fig. 4 shows the viscosity variation with shear rate for three different rheological models used in this study.

4. Governing Equations

A rigid wall tube with an axisymmetric local smooth circular constriction (sinusoidal profile) is considered. It is assumed that flow is laminar and incompressible and these conditions have no change during a period. The governing equations are as follows [24]:

$$\nabla . \vec{v} = 0 \tag{7}$$

$$r \left[\frac{\partial \vec{v}}{\partial t} + (\vec{v} . \nabla) \vec{v} \right] = -\nabla p + \nabla . \vec{t} \tag{8}$$

Where $\vec{t}$ is:

$$\vec{t} = h \vec{\dot{g}} = h \left[\nabla \vec{v} + (\nabla \vec{v})^{tr} \right] \tag{9}$$

Where h is constant for the Newtonian model and it can be determined by Eqs. (5) and (6) for non-Newtonian models.
The boundary conditions include no slip at the wall, no gradient or stress free at the outlet and symmetry at the centerline. Developed velocity profile with sinusoidal variation in each period (Eq. (2)) is used as a inlet boundary condition.
A validated user-enhanced finite volume code (teach-t) which benefits the advantage of boundary fitted coordinate system is used to solve the governing equations. The ability to solve two-dimensional flow field, unsteady and periodic problems, non-Newtonian fluid flow and fluid rheology simulation have been added to the code and the obtained predictions were verified by

numerical and experimental results [14] conceded the correctness of these enhancements.

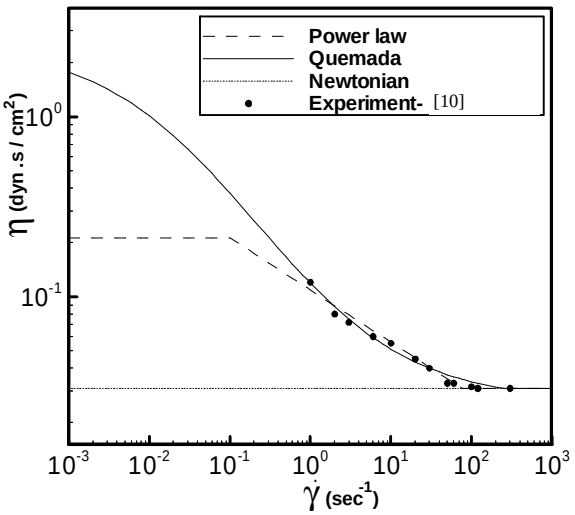

Fig. 4. Viscosity Variation vs. Shear rate Compared with Experimental Data.

5. Numerical Algorithm

The numerical computations used, is based on verified finite volume code algorithm [14,25] (teach-t) which has been modified to solve flow fields in irregular geometry with a boundary fitted coordinate system. The results presented in this paper are for 300×30 mesh size and repeated computations with finer meshes had no influence on the results and the mesh-independency of computations is revealed [14]. For eliminating of start-up unsteadiness of periodic flow it is necessary to carry out the computations at least for 3 or 4 periods. For the rheological and physical data which considered here maximum difference in results between the fourth and the fifth periods did not exceed 0.5% , therefore in this study the fourth period results have been presented as the final results. The number of time steps differs with the amount of Womersley number. The number of time steps (in each period) are 70, 180 and 490 for $Wo = 12.5, 7.5$ and 4.0 respectively. The computational work has been done on a PC machine with 1800 MHz Intel CPU and 256 MB DDR Ram. The total time for each computation depends on the Womersley number and rheology model varies from 36 hours to 6 days. The longest computation took place for the Quemada model at $Wo = 4$ and the shortest was belong to the Newtonian model at $Wo = 12.5$.

6. Assumptions

For obtaining following results the laminar incompressible flow in a rigid circular tube with a local smooth constriction is assumed. For the sake of simplicity the constriction profile and the input pulse profile are considered the sinusoidal. Besides, the blood density is assumed to be constant and three rheology models (Newtonian, Power law and Quemada) are employed to simulate blood rheology by estimating the apparent viscosity.

7. Verification

To ensure validity and correctness of the enhanced code, obtained results in two different cases including two-dimensional axisymmetric non-Newtonian/Newtonian steady flow in a sinusoidal stenosis and two-dimensional axisymmetric Newtonian pulsatile flow in a trapezoidal stenosis are verified with numerical [4] and experimental [5] results[14]. In this paper only the comparison of the pulsatile results are presented. Pulsatile results were computed for 45% stenosis with a trapezoidal profile (Fig.5) and sinusoidal pulsation (Eq. (2)) with mean Reynolds number of 575 and an amplitude variation of 360. The considered Womersley number is 7.5. Flow input waveform and three assumed time points for velocity profiles characterization are shown in Fig. 6.

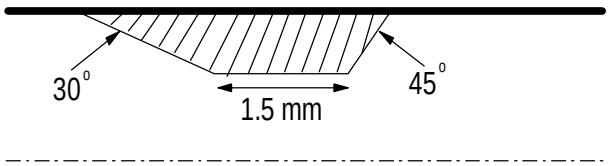

Fig. 5. Trapezoidal Stenosis Schematic.

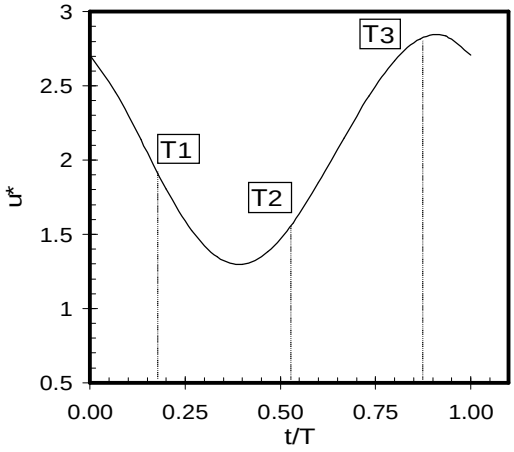

Fig. 6. Sinusoidal Pulsation of input Flow and three Assumed time Points for Velocity Profiles Description.

Measured and computed velocity profiles for three different time points are compared in Figs. 7-9. In all the figures presented in this paper u^*, r^* and z^* are non-dimensional velocity based on area-averaged velocity, non-dimensional radius based on tube radius and non-dimensional distance from mid-stenosis based on tube diameter respectively,

$$u^* = u/U \qquad (13\text{-a})$$

$$r^* = r/r_0 \qquad (13\text{-b})$$

$$z^* = z/D \qquad (13\text{-c})$$

For T_1 three velocity profiles at three different distances from mid-stenosis are plotted in Fig. 7. As T_1 is located in

decelerating portion of the flow, both computational and experimental results indicate separation at the wall for $z^* = 1$. Velocity profiles at T_2, near the lowest flow rate, correspond well with measured profiles for all axial locations (Fig. 8). For a location near the peak flow rate (T_3) velocity profiles are plotted in Fig. 9. At the first axial location, $z^* = 1$, the computed centerline velocity is less than the measured one. These discrepancies are due to the existence of an additional acceleration near the zenith of the experimental input pulse.For other axial location, $z^* = 2.5$ and 4.3, the predicted results match well with the experimental results.

8. Hemodynamic Wall Parameters

The goal of the hemodynamic definition is to achieve concise but useful information about disturbed blood flow and clearly elucidate the effects of the flow field. As mentioned, it is proved that hemodynamics parameters play important roles in access and progression of arterial diseases. Historically, the wall shear stress is one of hemodynamic parameters which is frequently used in disturbed blood flow as hemodynamic wall parameter [1]. Several widespread hypotheses exist like the (high) wall shear stress theory and the low (wall) shear stress theory based on the wall shear stress concept which link non-uniform hemodynamics with abnormal biological events and arterial progression shows the importance of the wall shear stress [1,3]. The high shear stress theory says that acute shear stresses may cause endothelial dysfunctions; hence, it may be responsible for local plaque formation. On the other hand, the low shear stress theory suggests that early atheroma occurs in low shear stress regions, not in high shear stress regions. Other arguments have been made that suggest the high wall shear stresses may be protective [1]. Time-averaged and non-dimensional hemodynamic wall parameters are considered here. The wall shear stress is defined as follows [1,10]:

$$WSS = \frac{1}{TrU^2}\int_0^T t_w dt \qquad (10)$$

In Eq. (10) the wall shear stress is expressed as time-averaged of the flow field force exerts on the arterial wall per unit area. In general for three-dimensional problems, t_w is a vector and WSS is calculated by integrated the magnitude of shear stress vector. But in a two-dimensional problem (like this study) t_w is a scalar value.

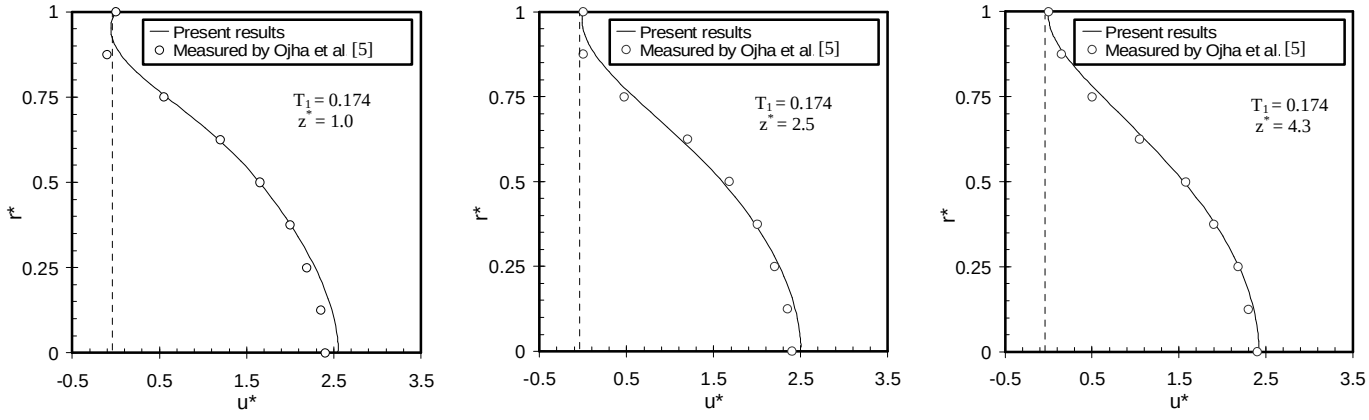

Fig. 7. Velocity Profiles in three Different Axial Locations at $T_1 = 0.174$.

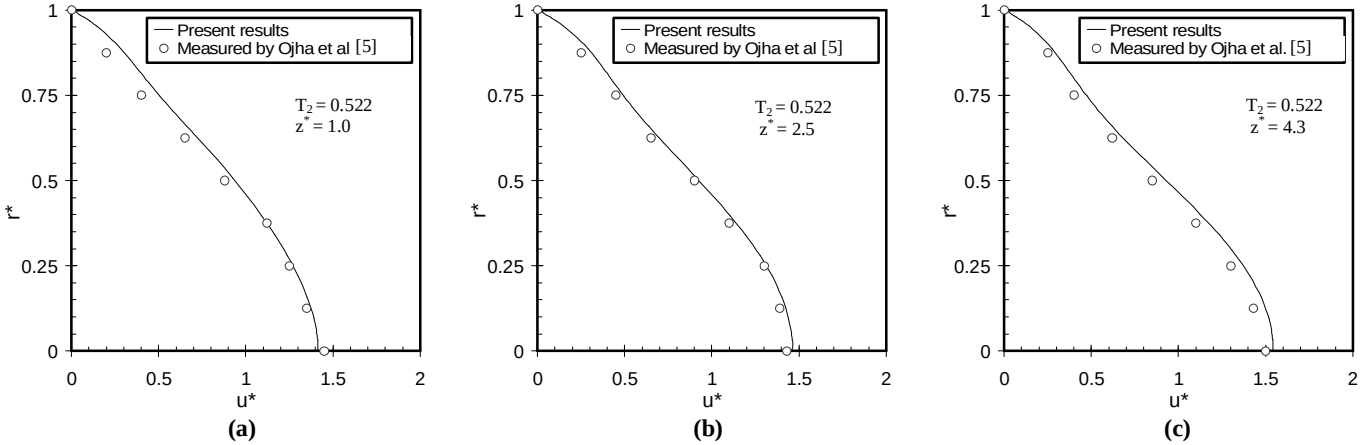

Fig. 8. Velocity Profiles in Three Different Axial Locations at $T_2 = 0.522$.

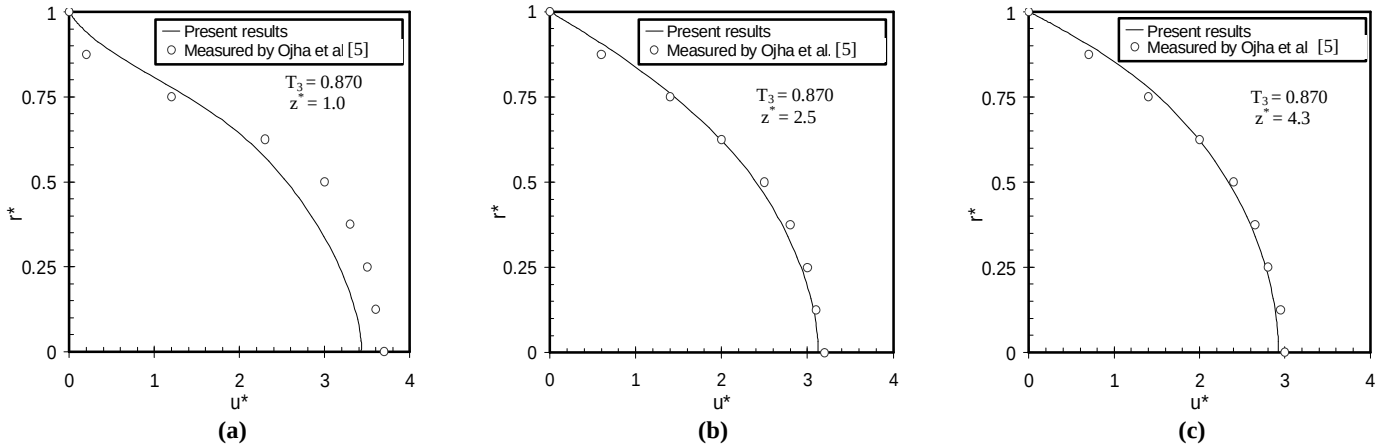

Fig. 9. Velocity Profiles in Three Different Axial Locations at $T_3 = 0.870$.

For indicating the changes in shearing forces, and hence 'aggravating effects' on the endothelium of arterial wall, the all shear stress gradient is used.

Furthermore, this parameter represents locally disturbed flow. The wall shear stress gradient is defined as [1,10]:

$$WSSG = \frac{D}{TrU^2}\int_0^T \left[\left(\frac{\partial t_w}{\partial s}\right)^2\right]^{1/2} \qquad (11)$$

Where s is the local coordinate along the wall. In Eqs. (10) and (11) T, r, U and D are period time, density, area-averaged velocity of mean Reynolds number and tube diameter respectively.

The final hemodynamic wall parameter is oscillatory shear index which characterizes the transient nature of vascular flow fields. The definition has recently been revised by He and Ku (cf. [1]) into a more usable form as [1, 10]:

$$OSI = \frac{1}{2}\left[1 - \frac{\left|\int_0^T t_w\, dt\right|}{\int_0^T |t_w|\, dt}\right] \qquad (12)$$

The OSI varies between 0 and 0.5 and is effective at locating points of time-averaged separation and reattachment [10]. The maximum of OSI shows the location time-averaged reattachment point in flow pattern. For the case of this study OSI has two maximum, one closely after mid point of stenosis and the another one far from the mid point. Near the mid point OSI increases because of decreasing flow area and increasing the velocity and its gradient. Therefore, the second maximum shows the location of time-averaged reattachment point.

9. Results and Discussion

The hemodynamic wall parameters for three Womersley numbers, $Wo = 12.5, 7.5$ and 4.0, are shown in Figs. 10-12. As mentioned before these parameters are the wall shear stress (WSS), the wall shear stress gradient ($WSSG$) and the oscillatory shear index (OSI).

Time-averaged reattachment points are clearly estimated by both WSS and OSI graphs. The axial location which WSS reaches to zero value (Figs. 10(a)-12(a)) or the location of second maximum value of OSI (Figs. 10 (c)-12(c)) show the time-averaged reattachment point for each models.

Time-averaged reattachment points for the models at three considered Womersley numbers are set in Table 2.

Time-averaged reattachment point shows the interaction of viscous and inertial forces and it differs upon the model. Reattachment point for the Newtonian and Power law models decreases with the Womersley number increasing while it is not monotonic for the Quemada model. In this model the longest time-averaged reattachment point appears at $Wo = 4.0$ and the shortest is belonging to $Wo = 7.5$. The time-averaged reattachment point is maximum for the Newtonian model and minimum for the Power law model at each Womersley number. But the Quemada model predicted time-averaged reattachment point is located between the Newtonian and Power law values.

Table. 2. The time Averaged Reattachment Points for Three Different Rheology Models

Wo	Newtonian	Power law	Quemada
4	4.175	2.891	3.056
7.5	3.813	2.792	2.858
12.5	3.122	2.628	2.957

The wall shear stress gradient shows the strength of the vertex which has been generated in the flow pattern.

The strength of primary vortex that is formed distal to the stenosis increases with the increase of the Womersley number (Figs. 10 (b)-12(b)). So fluid flow with the higher Womersley numbers generates stronger vortexes distal to the stenosis.

The vortex strength at each Womersley number has no considerable difference between three different rheology models.

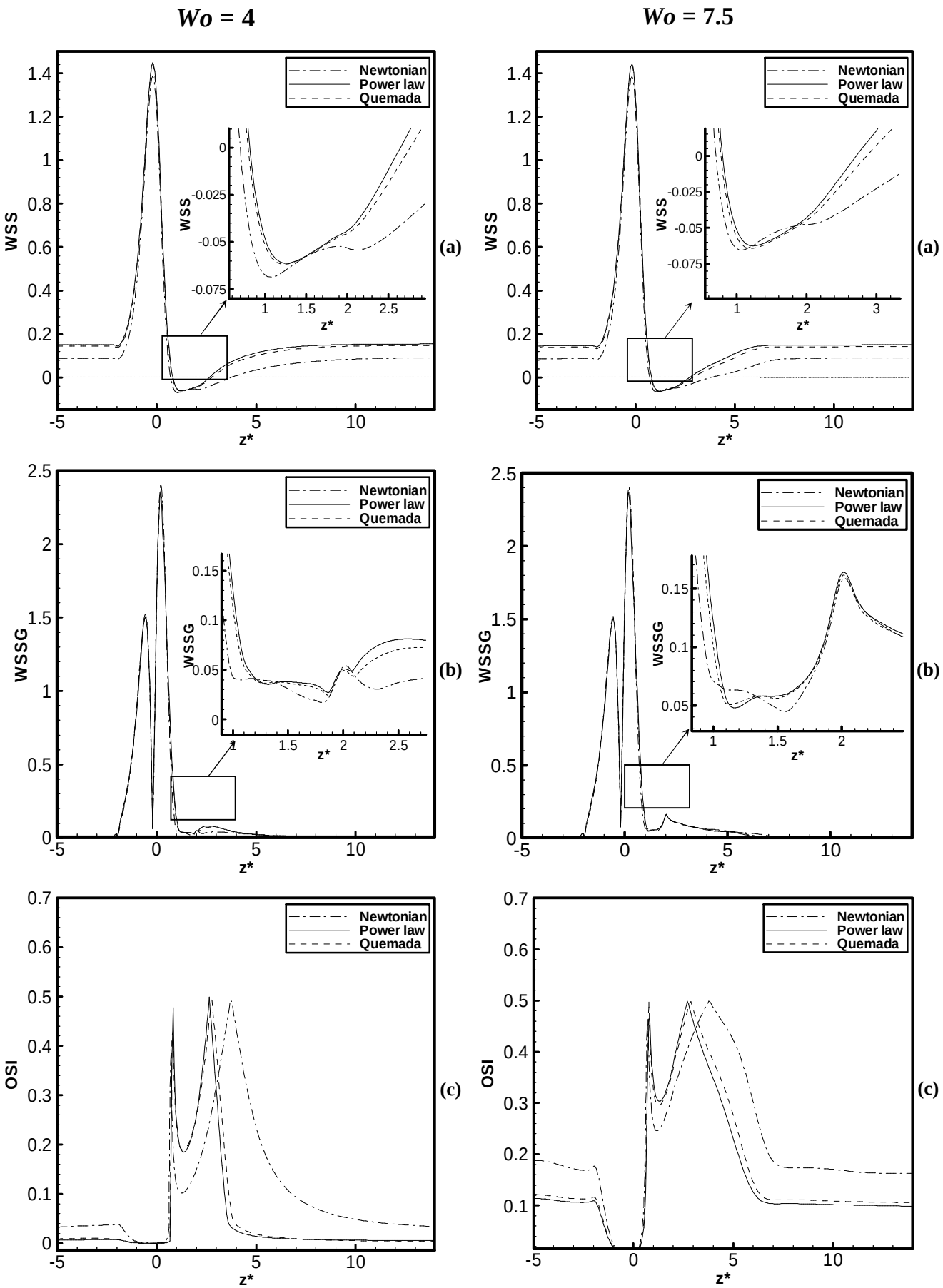

Fig. 10. Hemodynamic Wall Parameters at $Wo = 4$.

Fig. 11. Hemodynamic Wall Parameters at $Wo = 7.5$.

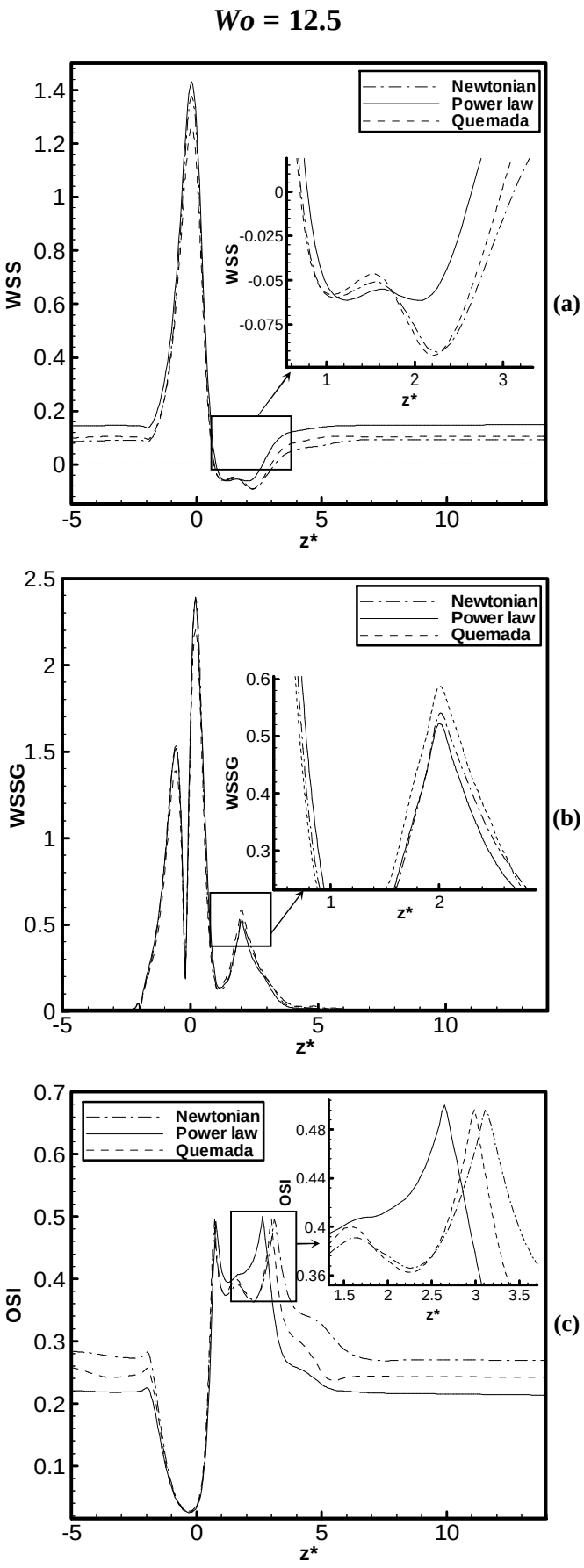

Fig. 12. Hemodynamic Wall Parameters at $Wo = 12.5$.

Figs. 10 (c)-12(c) show the OSI variation along the tube axial direction for $Wo = 12.5, 7.5$ and 4.0 respectively. For transient flow in a straight tube, the OSI indicates the portion of the cycle where the velocity profiles are reserved at the wall. As expected, the amount of OSI for locations proximal to the stenosis, which reserved flow is limited the decelerating phase of a period (for one inlet flow cycle), is less than locations which reserved flow occurs more during a cycle (like distal to and near the stenosis). Furthermore, it is predictable that because of higher viscosity of non-Newtonian models (than Newtonian viscosity) the non-Newtonian OSI values are less than Newtonian ones at the same axial locations.

10. Conclusion

The hemodynamic wall parameters at three Womersley numbers are computed and compared for three rheology models in the tubular flow with a smooth local occlusion and the following results are obtained:

1. The modified code can simulate blood flow in the vessels with axisymmetric stenosis accurately and would be able to use non-Newtonian models as blood rheology.
2. The maximum of time-averaged reattachment point is occurred at $Wo = 4.0$ for three rheology models. However, the time-averaged reattachment point decreases with the Womersley number for the both Newtonian and Power law models, but it is not monotonic for the Quemada model.
3. The Quemada time-averaged reattachment points are always located between the Newtonian model and the Power law model at the same Womersley numbers.
4. The strength of primary vortex which is located distal to the stenosis is similar for three rheology models.
5. The Quemada results, which are located between the Newtonian and The Power law results, are closer to the Power law model than the Newtonian model.
6. Qualitative comparison of the hemodynamic wall parameters graphs shows that the Power law model forms the upper bound, the Newtonian forms the lower bound and the Quemada model is located between two cases.

References

[1] Buchanan, Jr, J.R., Kleinstreuer, C., Truskey, G.A., Lei, M., "*Relation between non-uniform hemodynamics and sites of altered permeability and lesion growth at the rabbit aorto-celiac junction,*" Atherosclerosis, 143, 27-40, 1999.

[2] Kute, S.M., Vorp, D.A., "*The effect of proximal artery flow on the hemodynamics at the distal anastomosis of vascular bypass graft: computational study,*" Journal of Biomechanical Engineering, Vol. 123, 277, 2001.

[3] Hyun, S., Kleinstreuer, C., Archie Jr, J.P., "*Computational particle- hemodynamics analysis and geometric reconstruction after carotid endarterectomy,*" Computers in Biology and Medicine, 31, 365- 384, 2001.

[4] Tu, C., Deville, M., *"Pulsatile flow of non-Newtonian fluids through arterial stenoses,"* J. Biomechanics, Vol. 29, No. 7, 899-908, 1996.

[5] Ojha, M., Cobbold, R.S.C., Johnston, K.W., Hummel, R.L., *"Pulsatile flow through constricted tubes: an experimental investigation using photochromic tracer method,"* J. Fluid Mech., Vol. 203, 173-197, 1989.

[6] Kumar, B.V.R., Naidu, K.B., *"A pulsatile suspension flow simulation in a stenosed vessel,"* Math. Comput. Modelling , Vol. 23, No. 5, 75-86, 1996.

[7] Siouffi, M., Deplano, V., Pelissier, R., *"Experimental analysis of unsteady flows through a stenosis,"* Journal of Biomechanics, Vol. 31, 11-19, 1998.

[8] Ishikawa, T., Guimaraes, L.F.R., Oshima, S., Yamane, R., *"Effect of non-Newtonian property of blood on flow through a stenosed tube,"* Fluid Dynamics Research, Vol. 22, 251-264, 1998.

[9] Deplano, V., Siouffi, M., *"Experimental and numerical study of pulsatile flow through stenosis: wall shear stress analysis,"* Journal of Biomechanics, Vol. 32, 1081-1090, 1999.

[10] Buchanan, Jr, J.R., Kleinstreuer, C., Comer, J.K., *"Rheological effects on pulsatile hemodynamics in a stenosed tube,"* Computers & Fluids, Vol. 29, 695 -724, 2000.

[11] Ishikawa, T., Oshima, S., Yamane, R., *"Vortex enhancement in blood flow through stenosed and locally expanded tubes,"* Fluid Dynamics Research, Vol. 26, 35-52, 2000.

[12] Chakravarty, S., Mandal, P.K., *"Two-dimensional blood flow through tapered arteries under stenotic conditions,"* International Journal of non-Linear Mechanics, Vol. 35, 779-793, 2000

[13] Long, Q., Xu, X.Y., Ramnarine, K.V., Hoskins, P., *"Numerical investigation of physiologically realistic pulsatile flow through arterial stenosis,"* Journal of Biomechanics, Vol. 34, 1229-1242, 2001.

[14] Shahabi, P.B., *"Study of pulsatile blood flow in stenosed vessels,"* MSc thesis, Dept. of Mechanical Engineering, Ferdowsi University of Mashhad, Iran, 2003.

[15] Shahabi, P.B., Modarres Razavi, M.R., *"Pulsatile blood flow simulation in stenosed vessels by non-Newtonian fluid,"* Proceedings of 8th Fluid Mechanic Conference (in Persian), Tabriz University, Tabriz, Iran, September 2003.

[16] Modarres Razavi, M.R., Seyedein H., Shahabi, P.B., *"Study of pulsatile blood flow dynamic in stenosed vessels by non-Newtonian power law model,"* Submitted for review in International Journal of Science & Technology University of Iran (in Persian).

[17] Zhang, J.B., Kuang, Z.B., *"Study on blood constitutive parameters in different blood constitutive equation,"* Journal of Biomechanics, Vol. 33, 355-360, 2000.

[18] Fung, Y.C., *"Biomechanics (mechanical properties of living tissues),"* Spring- Verlag, New York, 1981.

[19] Pontrelli, G., *"Pulsatile blood flow in a pipe,"* Computers & Fluids, Vol. 27, No. 3, 367-380, 1998.

[20] Böhme, G., *"non-Newtonian fluid mechanics (North-Holland series in applied mathematics and mechanics; V.31),"* Elsevier Science Publisher B.V., 1987.

[21] Bae, H.O., Choe, H.J., *"Theory of non-Newtonian flow,"* Mathematics Subject Classification, 76A05, 1991.

[22] Chhabra, R.P., Richardson, J.F., *"non-Newtonian flow in the process industries,"* Butterworth-Heinemann, 1999.

[23] Bird, R.B., Stewart, W.E., Lightfoot, E.N., *"Transport phenomena,"* Second Edition, John Wily & Sons, Inc, 2002.

[24] Fletcher, C.A.J., *"Computational techniques for fluid dynamic 1- Specified Techniques for Different Flow Categories,"* Spring- Verlag, 1988.

[25] Seyedein, S.H., *"Simulation of fluid flow and heat transfer in impingement flows of various configurations,"* MS Thesis, Dept. of chemical Engineering, McGill University, 1993.

12. Nomenclature

D	Tube diameter
m	Constitutive coefficients of Power law model
n	Constitutive coefficients of Power law model
OSI	Oscillatory shear index
Re	Reynolds number
Re_{amp}	Amplitude Reynolds number
Re_{mean}	Mean Reynolds number
$R(z)$	Non-dimensional radius of stenosis based on tube radius
r^*	Non-dimensional radius based on tube radius
$r(z)$	Radius of stenosis

r_0	Tube constant radius
s	Local coordinate along the wall
T	Period time
t	Total time of blood flow
U	Inlet area averaged velocity
$U_{mean}(t)$	Center line velocity before stenosis
u^*	Non-dimensional velocity based on area-averaged velocity
$\vec{v}$	Velocity vector
Wo	Womersley number
WSS	Wall shear stress
$WSSG$	Wall shear stress gradient
z^*	Non-dimensional distance from mid-stenosis based on tube diameter
z_0	Stenosis half-length
d	Tube constricted thickness
$\dot{\gamma}$	Rate of strain tensor
$\dot{\gamma}$	shear rate (taken as the second scalar invariant of the rate of strain tensor)
η	Viscosity calculated from models
η_∞	Quemada constitutive coefficient
l	Quemada constitutive coefficient (shear rate modifier)
μ	Viscosity
μ_∞	Limiting high shear rate Newtonian viscosity
ν	Kinematic viscosity defined based on the Newtonian viscosity
ρ	Density
τ	Shear stress tensor
τ_0	Constitutive coefficient
τ_w	Wall shear stress tensor